DØ Note 6095-CONF

A search for the standard model Higgs boson in $H \to WW \to leptons + jets$ in 5.4 fb^{-1} of $p\bar{p}$ collisions at $\sqrt{s} = 1.96$ TeV

The DØ Collaboration
URL http://www-d0.fnal.gov
(Dated: July 21, 2010)

We present a new search for the standard model Higgs boson (H) in $p\bar{p}$ collisions at $\sqrt{s} = 1.96$ TeV, in topologies containing a charged lepton, an imbalance in transverse momentum ($\not\!\!E_T$), and jets, using an integrated luminosity of 5.4 fb^{-1} recorded with the D0 detector at the Fermilab Tevatron Collider. This analysis is sensitive primarily to contributions from Higgs bosons produced through gluon or weak-boson fusion, with subsequent decay $H \to WW \to \ell\bar{\nu}jj$, where $\ell = e$ or μ, and W represents a real or virtual W boson. In the absence of a signal, we set limits at 95% confidence on the production and decay of H into diboson final states for $\sigma(p\bar{p} \to H + X) \times B(H \to WW)$ for M_H in the range of 115–200 GeV/c^2. For $M_H = 165$ GeV/c^2, the observed and expected limits are factors of 5.5 and 3.8 larger than the SM value, respectively.

Preliminary Results for Summer 2010 Conferences

I. INTRODUCTION

The breaking of electroweak symmetry can be accommodated in the standard model (SM) through inclusion of a complex scalar "Higgs" field [1–4] that generates masses for the W and Z bosons, and possibly for all charged fermions. This further introduces a scalar Higgs boson (H) of unknown mass (M_H). The Higgs boson is the final prediction of the SM that has yet to be verified by experiment. Confirmation of its existence and properties would be a key step in elucidating the origins of electroweak symmetry breaking. For a Higgs boson with mass $M_H \gtrapprox 140\,\mathrm{GeV}/c^2$, the predominant decay mode is $H \to WW$, where one W must be virtual for $M_H < 2 \times m_W$. Previous searches [5, 6] in this channel have focused on dilepton final states $H \to WW \to \ell\bar{\nu}\bar{\ell}'\nu'$ ($\ell = e, \mu, \tau$) that also have significant missing transverse energy ($\not\!\!E_T$). This note presents the first search for production of the Higgs boson with subsequent decay including a single charged lepton. The data are taken from 5.4 fb^{-1} of $p\bar{p}$ collisions at $\sqrt{s} = 1.96\,\mathrm{TeV}$ recorded with the D0 detector [7] at the Fermilab Tevatron Collider. The largest cross section for producing SM Higgs bosons in $p\bar{p}$ collisions is the direct production of $H + X$ via gluon-gluon fusion processes, followed by the associated production with a vector boson and weak-boson fusion processes. The most striking signatures for a Higgs boson decaying into diboson pairs involve purely leptonic final states, including the "golden" mode, $H \to ZZ \to \ell\bar{\ell}\ell'\bar{\ell}'$, where the H can be reconstructed with greatest precision, in addition to the higher rate $H \to WW$, with both Ws decaying leptonically. However, small branching fractions limit the rates for all-leptonic final states. Decay channels containing a single charged lepton have more background, but their rates are also a factor of ≈ 6 higher than for the all-leptonic states. A recent analytical calculation of the full differential width for $H \to WW \to \ell\bar{\nu}jj$ decays [8] supports the important role of these channels for characterizing a potential standard model Higgs signature. The analysis reported here considers final state topologies with a single lepton (e or μ), two or more jets, and $\not\!\!E_T$, arising from $H \to WW \to \ell\bar{\nu}jj$. The primary backgrounds are from V+jets ($V = W, Z$), top, and diboson production and multijet events producing real or fake lepton signatures with $\not\!\!E_T$ arising from a mismeasurement of jet energies.

II. DATA AND SIMULATED SAMPLES

The D0 detector consists of tracking, calorimeter and muon systems. Charged particle tracks are reconstructed using silicon-microstrip tracking detectors and a scintillating fiber tracker, residing within a 2 T solenoid. Three uranium, liquid-argon calorimeters measure particle energies that are reconstructed into hadronic jets using an iterative midpoint cone algorithm with a cone radius, $R = 0.5$ [9]. Electrons and muons are identified through association of charged particle tracks with clusters in the electromagnetic sections of the calorimeters or with hits in the muon detector, respectively. The $\not\!\!E_T$ is reconstructed as the opposite of the vectorial sum of transverse components of energy depositions in the calorimeter and is corrected for any identified muons. Jet energies are calibrated using transverse momentum balance in photon+jet events [10], and the correction is propagated to the $\not\!\!E_T$. The data are recorded using triggers that are designed to select single leptons and, for the electron channel, also electron+jets final states. After imposing data quality requirements, the total integrated luminosity is 5.4 fb^{-1} [11].

Background contributions from most SM processes are determined through Monte Carlo (MC) simulation, while multijet (MJ) background is estimated from data. Events from W/Z+jets processes are generated with ALPGEN [12] and interfaced with PYTHIA [13] for modeling of parton evolution and hadronization. The p_T spectrum of the Z in the MC is reweighted to match that observed at D0 [14]. The p_T spectrum of the W is reweighted in the same manner, but corrected for differences between the p_T spectra of Z and W bosons predicted in next-to-next-to-leading order (NNLO) QCD [15]. The $t\bar{t}$ and electroweak single top-quark production backgrounds are simulated using ALPGEN and COMPHEP [16] generators, respectively, both interfaced to PYTHIA, while vector-boson pair production is generated entirely with PYTHIA. The $H \to WW$ signals are generated with PYTHIA for M_H from 115 to 200 GeV/c^2, in steps of 5 GeV/c^2. All these simulations use CTEQ6L1 parton distribution functions (PDF) [17].

The fractions of jets from heavy-flavor quarks in W/Z+jets events are obtained from MCFM [18]. Relative normalizations for W/Z+jets events are obtained from NNLO calculations of total cross sections [19], using the MRST2004 NNLO PDFs [20]. The absolute normalization for inclusive V+jets production is constrained further through a comparison with data, following a subtraction of other background sources. Cross sections for other SM backgrounds are taken from Ref. [21], or calculated with MCFM, and cross sections for signal are taken from Ref. [22].

Generated signal and background events are passed through a full GEANT3-based simulation [25] of detector response, and processed with the same reconstruction program used for data. Events from randomly selected beam crossings are overlaid on the simulated events to account for detector noise and contributions from the presence of additional $p\bar{p}$ interactions. Parameterizations of trigger efficiency for leptons are determined using decays of $Z \to \ell^+\ell^-$ [26]. The calibration of jet energy and its resolution are adjusted in simulated events to match what is observed in data.

III. EVENT SELECTION

Events in our signal sample are selected to contain candidates for $W \to \ell\nu$ decays in the final state by requiring $\not\!\!E_T > 15\,\text{GeV}$ and the presence of a lepton with $p_T > 15\,\text{GeV/c}$ that is isolated relative to jets, namely located outside jet cones, $\Delta R(\ell, \text{jet}) > 0.5$, where $(\Delta R)^2 = (\phi^\ell - \phi^{jet})^2 + (\eta^\ell - \eta^{jet})^2$, with ϕ being the azimuth and η the pseudorapidity [27]. The primary $p\bar{p}$ interaction vertex (PV) is required to be reconstructed within the longitudinal acceptance of the silicon vertex detector $|z_{\text{PV}}| < 60$ cm, where z is measured relative to the center of the detector along the beam direction. All leptons are required to originate from the PV, and to pass more restrictive isolation criteria based on other tracks and calorimeter energy deposited near the lepton trajectories. Electrons must also satisfy requirements on the spatial distribution of the shower, and timing information is applied to reject cosmic rays in the muon events. Leptons are required to be located within $|\eta_{det}| < 1.1$ for electrons and < 1.6 for muons, where η_{det} is the pseudorapidity calculated relative to the center, $z = 0$, of the detector. To reduce background from $Z \to \ell\ell$, top quark, and diboson decays, and to assure orthogonality to the dilepton channels, any event with an additional lepton is vetoed. We require two jets with $p_T > 20\,\text{GeV/c}$ and $|\eta_{jet}| < 2.5$. The jets are also required to originate from the measured PV. To suppress background from multijet events, we require events to have $m_T^W > 40 - 0.5 \times \not\!\!E_T$, where $m_T^W = \sqrt{(p_T^\ell + p_T^\nu)^2 - (\mathbf{p}_T^\ell + \mathbf{p}_T^\nu)^2}$ is the transverse mass of the W candidate.

Multijet background (MJ) in the electron channel is estimated from data using MJ enriched samples. In addition to the signal sample, we define a *loose* sample that does not require the more restrictive (*tight*) lepton isolation criteria to be satisfied and an *orthogonal* sample $N^e_{ortho.}$ satisfying the loose isolation criteria, but failing the tight criteria. The MJ background is based on this orthogonal sample. Both it and the loose sample contain multijet events where the jet shower fluctuated sufficiently to produce a false lepton and $\not\!\!E_T$, as well as W+jets events that fail the more restrictive isolation requirements. We can therefore subtract MC-simulated background from data and calculate the contribution from multijet background to the data that pass all selections, as follows. We define:

$$N_{loose} = N_W + N^e_{\text{MJ}} \tag{1}$$

$$N_{tight} = \epsilon_W \times N_W + \epsilon^e_{\text{MJ}} \times N^e_{\text{MJ}} \tag{2}$$

where $N_{loose/tight}$ is the number of events in data with the less/more restrictive lepton isolation requirements, N^e_{MJ} is the number of multijet events in the loose electron sample, ϵ_W is the conditional probability that an electron from W decay satisfying the loose isolation criteria the will also satisfy the tighter criteria, and ϵ^e_{MJ} is the corresponding probability for multijet events. We estimate ϵ_W from W+jets MC; ϵ^e_{MJ} is estimated from data, after subtracting all expected W decays from the both loose and tight samples, and is parameterized as a function of p_T^e, $\Delta\phi(e, \not\!\!E_T)$, and η^e_{det}. The MJ background in the signal sample is then estimated using $N^e_{ortho.}$, scaling events by the factor $\epsilon^e_{\text{MJ}}/(1 - \epsilon^e_{\text{MJ}})$ to correct for the presence of W decays.

To estimate the MJ contribution to the muon channel, we again define an orthogonal data sample $N^\mu_{ortho.}$ by reversing our tight isolation criteria for events that pass all other selections. The resulting orthogonal sample contains significantly fewer events than the electron channel and a different method is used to improve the modeling of multijet events. To correct for the presence of W events in $N^\mu_{ortho.}$, we examine six distributions: $\not\!\!E_T$, p_T^μ, $\Delta\phi(\mu, \not\!\!E_T)$, m_T^W, the p_T of the sub-leading jet, and the invariant mass of the dijet system, m^{jj}. The MJ background is modeled by the difference between $N^\mu_{ortho.}$ and MC from W/Z+jets, $t\bar{t}$, single top, and vector boson pair production ($N^{MC}_{ortho.}$). This correction is determined using bin-by-bin weights in each of the above distributions, calculated using:

$$f^{(d,i)}_{\text{MJ}} \times N^{\mu(d,i)}_{ortho.} = N^{\mu(d,i)}_{ortho.} - N^{MC(d,i)}_{otrho.} \tag{3}$$

where d is one of the six distributions, i is a bin index, and $f^{(d,i)}_{\text{MJ}}$ is the corresponding multijet weight. Each event in the orthogonal data is corrected using the average of six multijet weights to determine the best template for the distribution of events from multijet background. We estimate the total number of multijet events by fitting the p_T^μ and $\not\!\!E_T$ distributions in data to the isolated MC plus MJ template, with the normalizations for both V+jets and MJ (template) contributions as free parameters. To minimize any potential bias caused in determining the normalization for V+jets, the entire process is iterated after correcting this normalization. The resulting normalizations are found to be stable after a single iteration. Event yields for signal (for $M_H = 165\,\text{GeV}/c^2$) and background are listed in Table I.

IV. MULTIVARIATE ANALYSIS

We employ a random forest (RF) classifier to separate signal from background [28]. The RF is built from a collection of decision trees (DT), each trained on randomly selected subsamples from both signal and background MC events

TABLE I: Numbers of signal and background events expected after selection requirements. The signal corresponds to $M_H = 165\,\mathrm{GeV}/c^2$, V+jets includes W/Z plus light and heavy flavor jets after normalization to data, "top" includes pair and single top quark production, and VV stands for the sum of all diboson processes. The overall background normalization is fixed to the data after correcting the V+jets cross sections.

Channel	$H \to WW$	V+jets	Multijet	top	VV	data
electron	45.2	52156	11453	2433	1585	67627
muon	32.2	47201	2409	1598	1225	52433

and multijet background events from data. Each DT is trained using a set of ~ 30 discriminating variables such as reconstructed masses and momenta, angles between objects in the lab or in the reconstructed rest frame of the H boson, and combinations of variables such as event sphericity [13, 29], and relative p_T between specific objects. Potential variables are selected using a Kolmogorov-Smirnov test for differences in distributions between signal and background. This process is performed for three mass regions $M_H < 2 \times M_W, M_H \sim 2 \times M_W,$ and $M_H > 2 \times M_W$ to define an optimal set of variables to use for any M_H. The relative importance of individual variables depends on M_H. For example, variables associated with the four momenta of the two W bosons and of the WW system are increasingly sensitive at higher M_H values. A sample of input distributions for variables used in our decision trees is shown in Fig. 1.

The DT are constructed through successive splitting of signal and background contributions. A set of variables less than or equal to the total number of input distributions is selected and events are split into two nodes, one with enhanced signal and the other with enhanced background, according to the most effective discriminating variable. Each decision is controlled by minimization of an impurity criterion summed over the resulting two nodes, 2p(1-p), where p is the fraction of correctly classified events in each node. The process is repeated until no further optimization is possible or the number of events in a node falls below a minimal threshold of 500 events, reflecting the size of the MC samples used in this analysis. The RF is composed of 50 decision trees, and events are assigned a classification determined by the response averaged over all trees.

A random forest is trained separately for each channel and M_H 115–200 GeV/c^2 in steps of $5\,\mathrm{GeV}/c^2$. The outputs of the final RF discriminants are shown in Fig. 2 for M_H=165 GeV/c^2, for electron and muon channels. The RF output is computed with variable bin sizes chosen to limit statistical fluctuations in the MC background, thus introducing the apparent structures in the figure. The data are observed to be in agreement with expectations from standard-model backgrounds. Based on these RF output distributions, we set limits on the cross section for SM Higgs production.

V. LIMIT SETTING PROCEDURE

Upper limits on the production cross section multiplied by branching fractions $B(H \to WW)$ are determined using a CL_S modified-frequentist approach [30]. A test statistic is calculated based on the joint log-likelihood ratio (LLR) of the background-only and signal+background hypotheses, summed separately over all bins of the final discriminant in each channel. Systematic uncertainties affect both the number of selected events and the distributions in the final discriminants. Therefore to minimize degradation in signal sensitivity, both signal and background sources are fitted to the data by maximizing a likelihood function for both background-only and signal+background models, with the systematic uncertainties constrained through Gaussian priors on their probabilities [31].

VI. SYSTEMATIC UNCERTAINTIES

Systematic uncertainties used in deriving the cross section limits are listed in Table II. Experimental uncertainties arise from jet energy calibration and resolution, modeling of trigger efficiencies, jet reconstruction efficiency, lepton identification, estimation of the multijet background, and uncertainty on integrated luminosity. Systematic uncertainties may affect both the shapes and normalizations of the RF discriminant distributions for signal and background Those that preserve the normalization are listed as "shape only".

Theoretical uncertainties on cross sections for SM processes are taken from Ref. [21] and the heavy-flavor fractions for W/Z+jets production is estimated using MCFM. The uncertainties on cross sections for signal are taken from Ref. [22]. Because the overall cross section for (W/Z)+jets production is constrained by data, the uncertainty on its normalization is anti-correlated with the MJ background. The impact of theoretical uncertainties on the distributions of the final discriminants are accessed by varying the renormalization-and-factorization scale and by comparing ALPGEN interfaced with HERWIG [32] to ALPGEN interfaced with PYTHIA for (W/Z)+jets samples, and

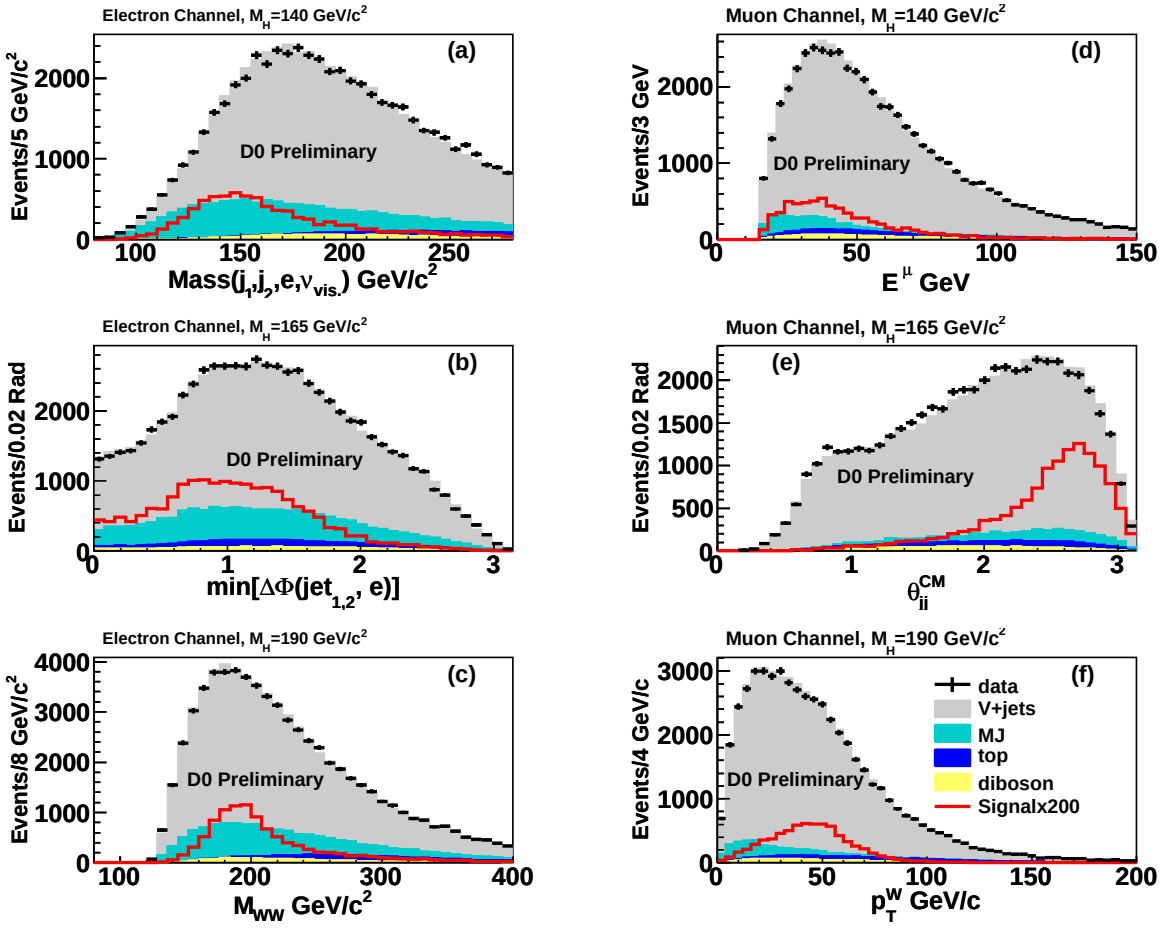

FIG. 1: Input distributions to DT for electron channel (a,b,c) and muon channel (d,e,f) compared to signal distributions for M_H=140, 165, and 190 GeV/c^2. (a) WW visible mass, M_{WW} reconstructed using only the transverse components of p_T^ν, (b) minimum azimuthal angle between the electron and either selected jet, (c) M_{WW} with estimated p_Z^ν, (d) energy of muon, (e) angle between the selected jets in the reconstructed Higgs center of mass frame (f) transverse momentum of the leptonically decaying W. The data are shown as points with error bars. The background contributions are shown as histograms, with sources indicated in the legend. Dibosons are labeled "VV", "top" includes pair and single top quark production., "V+jets" includes (W/Z)+(u, d, s, c, b, g) jets. The distributions for signal are multiplied by a factor of 200.

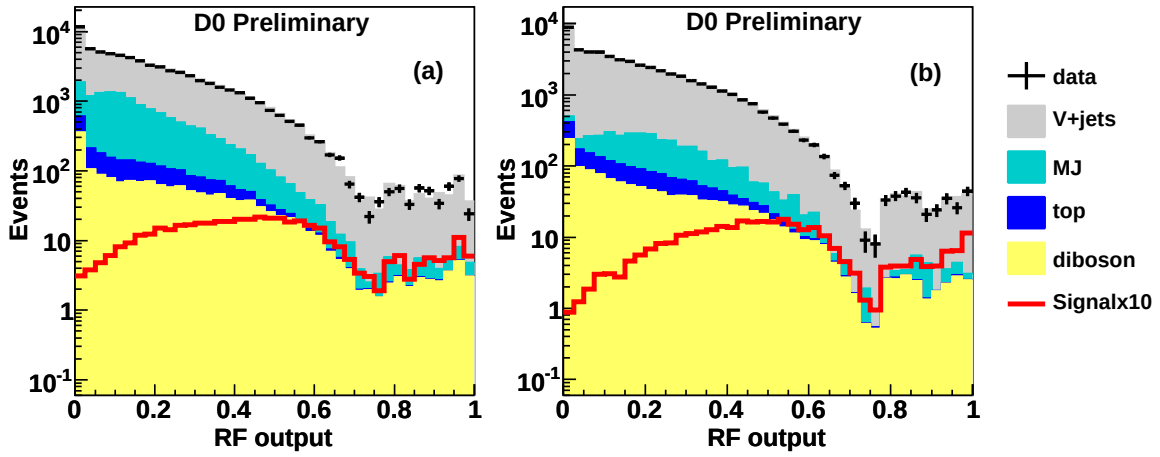

FIG. 2: Random forest outputs for $M_H = 165\,\mathrm{GeV}/c^2$: for the electron channel (a) and the muon channel (b). The data are shown as points with error bars. The background contributions are shown as histograms.

TABLE II: D0 Preliminary: Systematic uncertainties for electron and muon channels shown for $M_H = 165\,\mathrm{GeV}/c^2$. Uncertainties are listed as relative changes in normalization, in percent. Those affecting the shape of the RF discriminant are indicated with "Y".

Contribution	Shape	W+jets	Z+jets	Top	Diboson	$gg \to H$
Jet energy scale	Y	shape only	shape only	±6.0	$^{+3.3}_{-3.5}$	$^{+3.3}_{-2.0}$
Jet identification	Y	shape only	shape only	±3.3	±1.3	±3.5
Jet resolution	Y	shape only	shape only	$^{+0.5}_{-0.3}$	$^{+1.0}_{-0.5}$	$^{+2.0}_{-1.8}$
Association of jets with PV	Y	shape only	shape only	±3.8	±3.8	±4.8
Luminosty	-	-	±6.1	±6.1	±6.1	±6.1
Muon trigger	Y	±0.5	±0.5	±0.5	±0.25	±0.25
Electron identification	-	±4.0	±4.0	±4.0	±4.0	±4.0
Muon identification	-	±4.0	±4.0	±4.0	±4.0	±4.0
ALPGEN tuning	Y	shape only	shape only	-	-	-
Cross Section	-	±6.0	±6.0	±10.0	±7.0	±10.0
Heavy-flavor fraction	Y	±20	±20	-	-	-
PDF	Y	$^{+3.5}_{-2.5}$	$^{+8.0}_{-1.5}$	$^{+2.3}_{-3.6}$	±0.25	$^{+1.8}_{-3.8}$

		Multijet background	
		Electron channel	Muon channel
Multijet background	Y	±6.5	±26.2

TABLE III: D0 Preliminary: Ratios of the observed and expected exclusion limits relative to the SM production cross section multiplied by branching fraction for $H \to WW$, as a function of M_H.

M_H (GeV/c^2)	115	120	125	130	135	140	145	150	155
Observed	244.2	138.5	90.0	39.7	24.9	36.7	13.9	12.3	5.9
Expected	222.9	94.0	58.9	35.5	26.4	19.9	15.9	11.7	8.6
M_H (GeV/c^2)	160	165	170	175	180	185	190	195	200
Observed	4.1	3.8	4.0	5.5	14.9	16.8	22.4	19.2	16.1
Expected	5.2	5.5	6.3	7.5	8.8	10.3	11.5	11.3	12.1

varying the PDF models using the prescription of Ref. [17] for all MC samples. Correlations among systematic uncertainties in signal and background are taken into account in extracting the final results.

VII. RESULTS

The resulting limits are given in Table III. The limits and LLRs are shown in Fig. 3, as a function of M_H. The observed LLRs are within 1-2 standard deviations of the median of the LLR for the background-only hypothesis calculated with respect to statistical fluctuations and systematics variations.

For $M_H = 165\,\mathrm{GeV/c^2}$, the observed and expected limits on the combined cross section for Higgs production, multiplied by the branching fraction for $H \to WW$, are factors of 5.5 and 3.8 larger than the SM value, respectively. These are the first limits on standard-model Higgs production examining decays of the Higgs to two bosons having respective decays into a leptonic and a hadronic final state.

Acknowledgments

We thank the staffs at Fermilab and collaborating institutions, and acknowledge support from the DOE and NSF (USA); CEA and CNRS/IN2P3 (France); FASI, Rosatom and RFBR (Russia); CNPq, FAPERJ, FAPESP and FUNDUNESP (Brazil); DAE and DST (India); Colciencias (Colombia); CONACyT (Mexico); KRF and KOSEF (Korea); CONICET and UBACyT (Argentina); FOM (The Netherlands); STFC and the Royal Society (United Kingdom); MSMT and GACR (Czech Republic); CRC Program, CFI, NSERC and WestGrid Project (Canada);

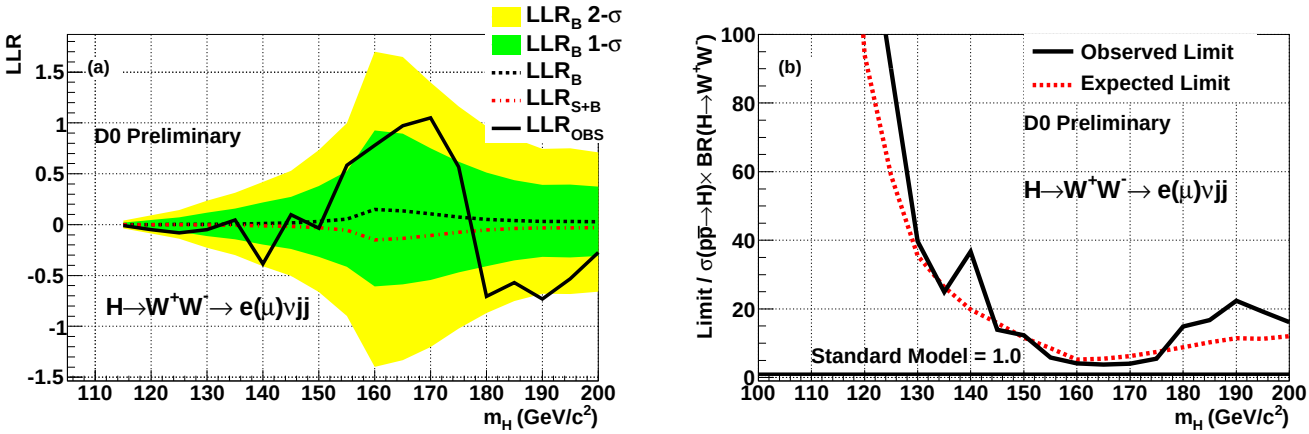

FIG. 3: (a) The observed LLR is shown as a solid line, the expected LLRs for the background-only and signal+background hypotheses are shown as dots and dashes, respectively, and the heavy and light shaded areas correspond to one and two standard deviations around the expected LLR for the background-only hypothesis. Positive values represent background-like fluctuations in the data. (b) Ratio of the 95% CL limit to the SM expectation as a function of M_H. Expected limits are shown by the dashed line, observed limits are shown by the solid line.

BMBF and DFG (Germany); SFI (Ireland); The Swedish Research Council (Sweden); and CAS and CNSF (China).

[1] P. W. Higgs, Phys. Rev. Lett. **13**, 508 (1964).
[2] F. Englert and R. Brout, Phys. Rev. Lett. **13**, 321 (1964).
[3] G. S. Guralnik, C. R. Hagen, and T. W. B. Kibble, Phys. Rev. Lett. **13**, 585 (1964).
[4] P. W. Higgs, Phys. Rev. **145**, 1156 (1966).
[5] V.M. Abazov *et al.* (D0 Collaboration), Phys. Rev. Lett. **104**, 061804 (2010); V.M. Abazov *et al.* (D0 Collaboration), Phys. Rev. Lett. **96**, 011801 (2006).
[6] T. Aaltonen et al. (CDF Collaboration), Phys. Rev. Lett. **104**, 061803 (2010); T. Aaltonen et al. (CDF Collaboration), Phys. Rev. Lett. **102**, 021802 (2009).
[7] V.M. Abazov *et al.* (D0 Collaboration), Nucl. Instrum. Methods in Phys. Res. A **565**, 463 (2006).
[8] B. Dobrescu and J. Lykken, JHEP **1004**, 083 (2010).
[9] G.C. Blazey *et al.*, FERMILAB-CONF-00-092-E (2000).
[10] V.M. Abazov *et al.*, (D0 Collaboration), Phys. Rev. Lett. **101**, 062001 (2008).
[11] T. Andeen *et al.*, FERMILAB-TM-2365 (2007).
[12] M.L. Mangano *et al.*, JHEP **0307**, 001 (2003); version 2.11 was used.
[13] T. Sjöstrand, S. Mrenna, and P. Skands, JHEP **0605**, 026 (2006); version 6.409 was used.
[14] V.M. Abazov *et al.*, (D0 Collaboration), Phys. Rev. Lett. **100**, 102002 (2008).
[15] K. Melnikov and F. Petriello, Phys. Rev. **D74**, 114017 (2006).
[16] E. Boos *et al.* (CompHEP Collaboration), Nucl. Instrum. Methods in Phys. Res. A **534**, 250 (2004).
[17] J. Pumplin *et al.*, JHEP **0207**, 012 (2002); D. Stump *et al.*, JHEP **0310**, 046 (2003).
[18] J.M. Campbell and R.K. Ellis, Phys. Rev. D **60**, 113006 (1999).
[19] R. Hamberg, W.L. van Neerven, and W.B. Kilgore, Nucl. Phys. **B359**, 343 (1991), *ibid.* **B644**, 403 (2002) [erratum].
[20] A.D. Martin, R.G. Roberts, W.J. Stirling, and R.S. Thorne, Phys. Lett. B **604**, 61 (2004).
[21] M. Cacciari *et al.*, JHEP **404**, 068 (2004); N. Kidonakis and R. Vogt, Phys. Rev. D **68**, 114014 (2003); N. Kidonakis, Phys. Rev. D **74**, 114012 (2006).
[22] T. Hahn *et al.*, `arXiv:hep-ph/0607308` (2006).
[23] S. Frixione and B.R. Webber, JHEP **0206**, 029 (2002).
[24] T. Gleisberg et al., JHEP 0402, 056 (2004).
[25] R. Brun and F. Carminati, CERN Program Library Long Writeup W5013, 1993 (unpublished).
[26] V.M. Abazov *et al.*, (D0 Collaboration), Phys. Rev. D. **76**, 012003 (2007).
[27] The pseudorapidity is defined as $\eta = -\ln[\tan(\theta/2)]$, where θ is the polar angle with respect to the proton beam direction.
[28] L. Breiman, Random Forests, Machine Learning **45**, 5-32 (2001).
[29] J.D. Bjorken and S.J. Brodsky, Phys. Rev. D. **1**, 1416 (1970).
[30] T. Junk, Nucl. Instrum. Methods in Phys. Res. A **434**, 435 (1999); A. Read, J. Phys. G **28**, 2693 (2002).
[31] W. Fisher, FERMILAB-TM-2386-E.

[32] G. Corcella *et al.*, JHEP **0101**, 010 (2001).